FLOW- INDUCED MICROSTRUCTURE OF A SYNTHETIC MESOPHASE PITCH

D.Grecov , Department of Mechanical Engineering, University of British Columbia, 2054-6250 Applied Science Lane, Vancouver, BC, Canada V6T 1Z4
S. Kundu [(1)], A. A. Ogale, Department of Chemical Engineering, Center for Advanced Engineering Fibers and Films, 203 Earle Hall, Clemson University, Clemson, SC 29634
A.D. Rey, Department of Chemical Engineering, McGill University, 3610 University Street, Montreal, Quebec, Canada H3A 2B2

Abstract

Carbon products derived from mesophase pitch exhibit high stiffness and thermal conductivity because of the high degree of molecular orientation. The internal structure and final properties of such products are highly dependent on the flow-induced microstructure developed during melt processing. By developing an experimental protocol to preserve the rheological samples, microstructural features were measured from the same mesophase specimens as those used for rheological testing. In steady shear flow, the microstructure was flow-aligned, and similar to the fibrous structure reported in the literature. Transient stress responses displayed a non-monotonic behaviour and microscopic observations indicate that the local maximum in the shear stress is likely caused by the yielding of the initial microstructure. To develop a fundamental understanding of these complex flow dynamics, a multiscale model based on Landau-de Gennes theory was adapted for discotic liquid crystalline materials. A validation of the simulation results with the experimental data has been performed and qualitatively agreements to all observed phenomena have been found. Based on experiments and numerical simulations, we provide a systematic understanding of flow-microstructure relationships during transient and steady shear flow.

1. Introduction

Carbon fibers produced from mesophase pitch exhibit high stiffness and thermal conductivity and are used in satellite structures and other thermal management applications. The internal structure and therefore the final properties of pitch-based carbon fibers are highly dependent on the flow-induced microstructure developed during the melt-spinning process. Improvements in carbon fiber quality require a better understanding of the flow and microstructural behavior of mesophase pitches.

Natural and synthetic mesophase pitches are discotic nematic liquid crystals (DNLCs) and precursor material used in the manufacturing of high-performance carbon fibers, by the melt spinning process (Edie, 2003). The discotic nematic liquid crystals consists of flat, disk-like molecules more or less aligned along a common direction, represented by the uniaxial director **n** (the average orientation of the unit normals to the disk-like molecules).

The shear flow behaviour and rheology of DNLCs depend on the sign and magnitude of the reactive parameter λ, which is the ratio of the flow aligning effect of the deformation rate and the tumbling (rotational) effect of the vorticity. For DNLCs, $\lambda < -1$ and hence they display the flow-aligning mode. At present there is strong evidence that carbonaceous mesophases are flow-aligning systems, since mesophase fibers showed clearly ordered macroscopic orientation in the experiments.

Textures are spatial distributions of defects. Inversion walls are 2D non-singular defects, in which spatially localized director gradients occur. In this paper we use shear-induced generation of splay-bend inversion walls as a model for texture generation. Models and theories of nucleation and coarsening of textures under flow is a topic of current interest (Tsuji and Rey, 1997), (Singh and Rey, 2000), (Grecov and Rey, 2003). The anisotropic properties of nematics give rise to novel field-induced re-orientation mechanisms and defect nucleation (Rey, 1990). Typically inversion walls in NLCs under external fields arise because two equivalent re-orientation (rotation) mechanisms are possible. The net result is a field-aligned sample with trapped thin layers that separate regions of clockwise rotations from those of anti-clockwise rotation.

The main impact of molecular weight on rheology is embodied in the Deborah number (De), or ratio of molecular time scale to flow time scale. For low-molecular weight carbonaceous mesophases the Deborah number is less than one and hence molecular elasticity can be neglected, and only the orientation process is relevant.

This work uses a very well established mesoscopic model for liquid crystalline materials is based on the Landau-de Gennes free energy (deGennes, 1993), (Rey and Denn, 2002). This model takes into account all the three major effects (short and long range order elasticity and viscous flow) and can capture general and complex phenomena of liquid crystals behavior (e.g. banded texture, defect generation and coarsening phenomena) which are not captured by the classical theories.

(1) Present address: University of Massachusetts- Amherst, PSE department

Similar to other thermotropic liquid crystals, mesophase pitches are anisotropic viscoelastic textured materials whose rheological properties depend on deformation rates and textural features. Numerous studies (Larson and Mead, 1992, De'Neve et al., 1993, Ugaz and Burghardt, 1998) have been performed on liquid-crystalline polymers to understand the evolution of microstructure and orientation by optical microscopy and X-ray diffraction (Picken et al., 1990, Mather et al., 2000, Guo et al., 2005). *In situ* studies on structure measurement have been performed using optical microscopy coupled with a shearing hot-stage (Mather et al., 2000). The transparent/translucent nature of the liquid crystalline polymers enables real-time measurement of evolution of domain structure and defect dynamics by optical microscopy in the transmission mode. Unfortunately, due to the opacity of pitch, such real-time microscopic studies can not be performed on mesophase pitches.

Offline, reflected-mode optical microscopy on solidified pitch samples has been used to characterize the microstructure of mesophase pitch. The effect of shear flow on the microstructure of mesophase pitch has been studied in literature (Fleurot and Edie, 1998, Cato and Edie, 2003). It was reported that, domain size decreased with increasing shear rates, and the size approximately followed the Marrucci's polydomain theory for LCPs (Marrucci, 1984).

Rheological behavior at low-medium shear rates can be studied using the cone-plate geometry. Although high shear rates cannot be generated in this geometry, it is a valuable technique for generating homogeneous (constant) shear rate and shear stress within the entire flow. Consequently, this geometry has been used for rheological characterization of several thermotropic liquid crystalline materials (De'Neve et al., 1993) and mesophase pitch (Cato and Edie, 2003). However, the microstructure development in mesophase pitch during flow startup and transient state has not been extensively reported in the literature.

This paper summarizes recent advances in our understanding of the relationship between mesophase structure and flow. The results show that the model accurately predicts the formation of mesophase structure during processing and explains the experimental observations. Therefore, the objective of this study is to assess the microstructure evolution with time/strain for a synthetic mesophase pitch (AR-HP), to provide a comprehensive structural and rheological study of mesophase pitch.

2. Experimental

A naphthalene-derived, synthetic mesophase pitch (AR-HP grade, Mitsubishi Gas Chemical Company) with a softening point of 285±5°C [MSDS, CAS No. 25135-16-4, Mitsubishi Gas Chemical Company) was used throughout the study. The transient rheological experiments were conducted at 297°C in an inert N_2 environment on TA Instruments ARES rheometer (TA Instruments Inc.) using a cone-plate fixture of 25 mm diameter with a cone angle of 0.1 rad. The rheological experiments were performed on vacuum-pelletized cylindrical samples (Kundu and Ogale 2006).

By developing an experimental protocol to preserve the rheological samples, microstructural features were obtained from the same mesophase pitch specimens as those used for rheological testing (Kundu and Ogale, 2006). As shown earlier, the microstructure was studied in three orthogonal sections: AA′ section (r-ϕ or vorticity-flow section), BB′ (r-θ or vorticity-gradient section) and CC′ (θ–ϕ or gradient-flow section). Both rheological experiments and microstructural studies were repeated at least three times to check the consistency. For microstructure identification, pyrolytic graphite sample deposited around a PAN-based carbon fiber was used. The details of different color could be found in an earlier study (Kundu and Ogale, 2006). The image analysis was performed by using ImagePro® software.

3. Theory

A Landau-de Gennes model that takes into account short range and long range energy, and flow-induced orientations has been adapted to describe the flow behaviour of flow-aligning thermotropic discotic nematic liquid crystals as models of carbonaceous mesophases . The dynamics of the tensor order parameter is given by the following sum of flow **F**, short range $\mathbf{H}^{sr}$, and long range $\mathbf{H}^{lr}$ contributions (Grecov and Rey, 2002):

$$\hat{\mathbf{Q}} = \mathbf{F}(\mathbf{Q},\nabla\mathbf{v}) + \mathbf{H};\quad \mathbf{H} = \mathbf{H}^{sr}\left(\mathbf{Q},\overline{D}_r(\mathbf{Q})\right) + \mathbf{H}^{lr}(\nabla\mathbf{Q}) \tag{1}$$

(i) flow contribution **F**:

$$\mathbf{F}(\mathbf{Q},\nabla\mathbf{v}) = \tfrac{2}{3}\beta\mathbf{A} + \beta\left[\mathbf{A}\cdot\mathbf{Q} + \mathbf{Q}\cdot\mathbf{A} - \tfrac{2}{3}(\mathbf{A}:\mathbf{Q})\mathbf{I}\right] - \tfrac{1}{2}\beta\left[(\mathbf{A}:\mathbf{Q})\mathbf{Q} + \mathbf{A}\cdot\mathbf{Q}\cdot\mathbf{Q} + \mathbf{Q}\cdot\mathbf{A}\cdot\mathbf{Q} + \mathbf{Q}\cdot\mathbf{Q}\cdot\mathbf{A} - \{(\mathbf{Q}\cdot\mathbf{Q}):\mathbf{A}\}\mathbf{I}\right] \tag{2}$$

(ii) short-range elastic contribution $\mathbf{H}^{sr}$:

$$\mathbf{H}^{sr}\left(\mathbf{Q},\overline{D}_r(\mathbf{Q})\right) = -6\overline{D}_r\left[(1-\tfrac{1}{3}U)\mathbf{Q} - U\mathbf{Q}\cdot\mathbf{Q} + U\{(\mathbf{Q}:\mathbf{Q})\mathbf{Q} + \tfrac{1}{3}(\mathbf{Q}:\mathbf{Q})\mathbf{I}\}\right] \tag{3}$$

(iii) long-range elastic contribution $\mathbf{H}^{lr}$:

$$\mathbf{H}^{lr}(\mathbf{Q}) = 6\overline{D}_r\left[\frac{L_1}{2ckT}\nabla^2\mathbf{Q} + \frac{1}{2}\frac{L_2}{c\kappa T}\left[\nabla(\nabla\cdot\mathbf{Q}) + \{\nabla(\nabla\cdot\mathbf{Q})\}^T - \tfrac{2}{3}\mathrm{tr}\{\nabla(\nabla\cdot\mathbf{Q})\}\mathbf{I}\right]\right] \tag{4}$$

$$\overline{D}_r = \frac{Dr}{\left(1-\frac{3}{2}\mathbf{Q}:\mathbf{Q}\right)} \tag{5}$$

Here **A**, L_i (i=1,2), U and β are the rate of deformation tensor, the Landau coefficients, the nematic potential and the molecular shape parameter, respectively. The dimensionless numbers Er (Ericksen number) and energy ratio R:

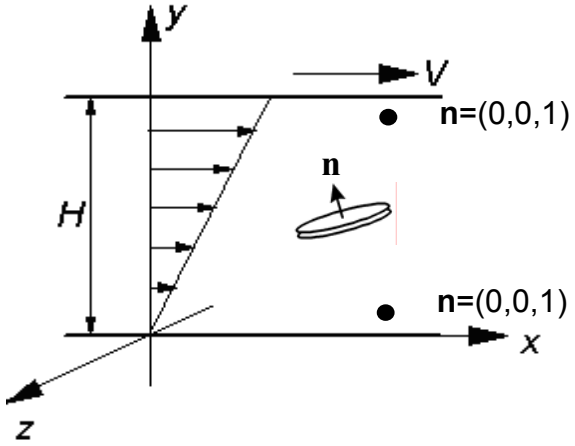

Figure 1. Definition of the flow geometry and coordinates system for simple shear flow. The lower plate is at rest and the upper plate moves in the x- direction with a constant velocity V. H is the gap separation.

$$\mathrm{Er} = \frac{\dot{\gamma}H^2ckT^*}{2L_1D_r} \qquad \mathrm{R} = \frac{3H^2ckT^*}{L_1} \tag{6a,b}$$

give the ratio of viscous flow effects to long-range order elasticity, and short-range order elasticity to long-range order elasticity, respectively (H is the characteristic distance between the two plates (see figure 1) , V is the constant velocity of the top plate and T^* is the isotropic-nematic transition temperature).

A unified expression for the extra stress tensor is used. The total extra stress tensor $\mathbf{t}^{t}$ for liquid crystalline materials is given by the sum of symmetric viscoelastic stress tensor $\mathbf{t}^{s}$, anti-symmetric stress tensor, and Ericksen stress tensor $\mathbf{t}^{Er}$:

$$\mathbf{t}^{t} = \mathbf{t}^{s} + \mathbf{t}^{a} + \mathbf{t}^{Er} \tag{7}$$

The symmetric visco-elastic stress tensor $\mathbf{t}^{s}$ is expressed as a sum of a symmetric viscous stress contribution $\mathbf{t}^{v}$ and an elastic stress contribution $\mathbf{t}^{e}$ (Farhoudi and Rey, 1993) as:

$$\mathbf{t}^{s} = \mathbf{t}^{v} + \mathbf{t}^{e} \tag{8}$$

The stress contribution $\mathbf{t}^{v}$ found is given by:

$$\begin{aligned}\mathbf{t}^{v} &= \nu_1\mathbf{A} + \nu_2\{\mathbf{Q}\cdot\mathbf{A} + \mathbf{A}\cdot\mathbf{Q} - \tfrac{2}{3}(\mathbf{Q}:\mathbf{A})\mathbf{I}\} + \\ &\nu_4\left[(\mathbf{A}:\mathbf{Q})\mathbf{Q} + \mathbf{A}\cdot\mathbf{Q}\cdot\mathbf{Q} + \mathbf{Q}\cdot\mathbf{A}\cdot\mathbf{Q} + \mathbf{Q}\cdot\mathbf{Q}\cdot\mathbf{A} + \{(\mathbf{Q}\cdot\mathbf{Q}):\mathbf{A}\}\mathbf{I}\right]\end{aligned} \tag{9}$$

where ν_1, ν_2, ν_4 are viscosities coefficients. Characteristic values for these viscosities coefficients for discotic nematic liquid crystals can be found by mapping the total stress tensor with the stress tensor given by the Leslie-Ericksen vector theory. The elastic contribution $\mathbf{t}^{e}$ that couples stress to the molecular field **H** is given as:

$$\begin{aligned}\mathbf{t}^{e} &= (ckT)[-\frac{2}{3}\beta\,\mathbf{H} - \beta\left\{\mathbf{H}\cdot\mathbf{Q} + \mathbf{Q}\cdot\mathbf{H} - \frac{2}{3}(\mathbf{H}:\mathbf{Q})\mathbf{I}\right\} \\ &+ \frac{1}{2}\beta[(\mathbf{H}:\mathbf{Q})\mathbf{Q} + \mathbf{H}\cdot\mathbf{Q}\cdot\mathbf{Q} + \mathbf{Q}\cdot\mathbf{H}\cdot\mathbf{Q} + \mathbf{Q}\cdot\mathbf{Q}\cdot\mathbf{H} - \{(\mathbf{Q}\cdot\mathbf{Q}):\mathbf{H}\}\mathbf{I}]]\end{aligned} \tag{10}$$

The antisymmetric contribution $\mathbf{t}^{a}$ arises whenever **H.Q** is not symmetric, and is given as (Farhoudi and Rey, 1993):

$$\mathbf{t}^{a} = ckT(\mathbf{H}\cdot\mathbf{Q} - \mathbf{Q}\cdot\mathbf{H}) \tag{11}$$

The Ericksen stress contribution $\mathbf{t}^{Er}$ arises from the long range elasticity and is given as:

$$\mathbf{t}^{Er} = -\frac{\partial f}{\partial\nabla\mathbf{Q}} : (\nabla\mathbf{Q})^{T} = \left[-L_1\nabla\mathbf{Q} : (\nabla\mathbf{Q})^{T} - L_2(\nabla\cdot\mathbf{Q})\cdot(\nabla\cdot\mathbf{Q})^{T}\right] \tag{12}$$

The dimensionless first normal stress difference (N_1^*) and the dimensionless apparent shear viscosity (η^*) used to characterize the steady shear rheological material functions are given by:

$$N_1^* = t_{xx}^* - t_{yy}^* = \frac{t_{xx} - t_{yy}}{ckT^*} \tag{13}$$

$$\eta^* = \frac{t_{yx}}{\dot{\gamma}}\cdot\frac{6Dr}{ckT^*} \tag{14}$$

4. Results and Discussion

The model equations are a set of five coupled non-linear parabolic partial differential equations. The equations are solved using Galerkin Finite Elements for spatial discretization and a forth order Runge-Kutta time adaptive method. The selected adaptive time integration scheme is able to efficiently take into account the stiffness that rises due to the disparity between time scales and length scales.

In this work we study a rectilinear simple start-up shear flow with Cartesian coordinates, fixed boundary conditions are used, such that the director **n** is anchored along the vorticity direction, as shown in figure1. The initial director field is oriented in x-z plane, with $80<\phi<100$ degrees (ϕ is the twist angle and ϕ=90 degrees corresponds to the vorticity direction) with random variation. In the present work the parametric values are set at: U=3.5,β =-1.2 (flow aligning system), and the simulations are performed for a range: $10^4<Er<3x10^6$ ($0.01<De<3$) and for $R=10^6$.

It is found that as the shear-rate increases, the pathway between an oriented non-planar state and an oriented planar state is through texture formation and coarsening. The shear-rate dependent dimensionless

numbers that control the texture formation and coarsening process is Ericksen Er as Deborah number, De <1. The emergence of texture is independent of the Deborah number, and occurs at $Er=10^4$.

The nucleation of the parallel array of splay-bend inversion walls is due to the degeneracy in reorientation towards the shear plane. Increasing the Ericksen number, the number of the splay-bend walls increases (see figure 3b). Here the spatial variations of the director occur over length scales much smaller than the thickness of the sample H and number of walls is high and time dependent, so they can be described in a statistical manner.

Figure 2a shows a computed gray scale visualization of director component n_z ($0 \leq y^* \leq 1$) as a function of strain for Er=10000. The figure shows a typical example of two splay-bend inversion walls in the bulk. Figure 2b shows the steady state director components (n_x, n_y and n_z) as a function of dimensionless distance y*, corresponding to figure 3a. At these relatively low Er no coarsening takes place and the director is periodic.

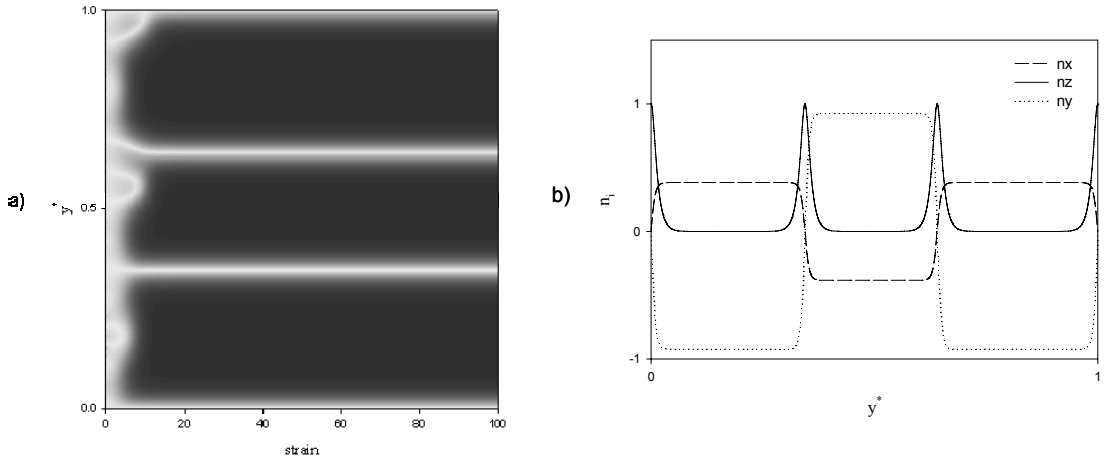

Figure 2. a) Computed grey scale visualization of director component n_z ($0 \leq y^* \leq 1$) as a function of strain (γ) Black -in plane orientation (n_z=0) and light - orientation along the vorticity (n_z=1) for Er=10000; b) Steady state director components (n_x, n_y, n_z) as a function of dimensionless distance y*.

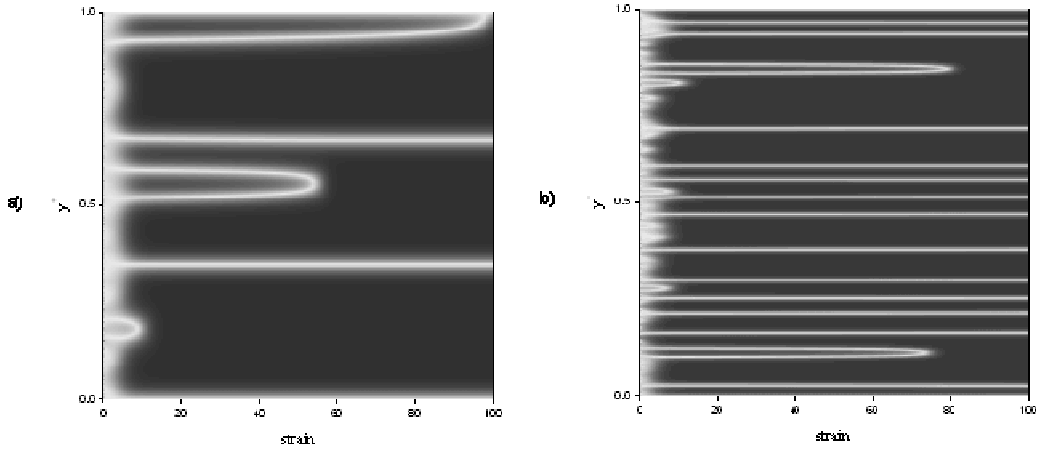

Figure 3. Computed grey scale visualization of director component n_z ($0 \leq y^* \leq 1$) as a function of strain (γ). Black -in plane orientation (n_z=0) and light- orientation along the vorticity (n_z=1): a) $Er=4x10^4$; b) $Er=2.4x10^5$.

By increasing the shear rate (Ericksen number), the number of splay-bend walls increases (see figure 3). The steady state texture of a liquid crystal is given by the balance of nucleation and coarsening processes. Coarsening events limit the lifetime of an inversion wall, and a texture can be viewed as a balance between birth-death events.

Figure 3 represents computed grey scale visualizations of director component n_z ($0 \leq y^* \leq 1$) as a function of strain for a) $Er=4x10^4$ ($De=0.04$) and b) $Er=2.4x10^5$ ($De=0.24$). At this relatively low Ericksen numbers, splay-bend walls can annihilate by two mechanisms: wall-wall annihilations (figure 3a,b) and wall-bounding surface reaction (figure 3a) .

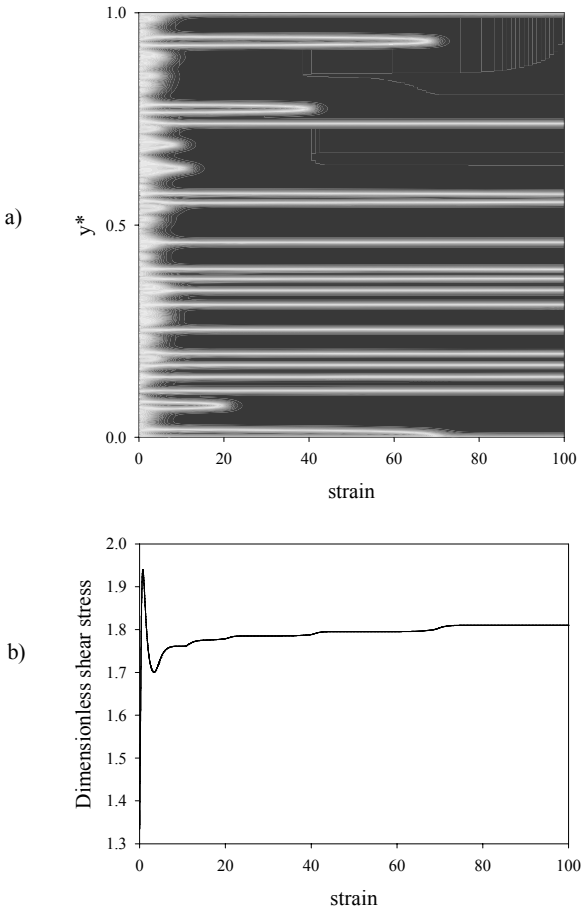

Figure4. a) Computed grey scale visualization of director component n_z ($0 \leq y^* \leq 1$) as a function of strain.
b) Dimensionless shear stress τ as a function of strain.

Next we present the transient evolution of the shear stress in order to establish the impact of textural transformations on the transient shear rheology. Figure 4a shows computed grey scale visualization of director component n_z ($0 \leq y^* \leq 1$) as a function of strain. Black represents in-plane orientation ($n_z=0$) and light represents orientation along the vorticity axis ($n_z=1$): for $Er=3x10^5$, $R=10^6$, $1/U=0.28$. Texture evolution presents the two defect annihilation mechanisms (wall-wall and wall-bounding surface). Figure 4b shows the transient evolution of the dimensionless shear stress as function of strain corresponding to Figure 4a. The shear stress evolution shows an overshoot (1 strain units) and an undershoot (4 strain units) followed by a plateau. The shear stress evolution is affected by the out-of-plane $\rightarrow$ in plane orientation change (undershoot) and the in plane re-orientation (overshoot). When two walls or a wall with the bounding surface

interact, a step-like shear stress increase occurs. The steady state is achieved in approximately 100 units strain. The shear stress response to shear start-up is in qualitative agreement with experimental observations (see fig. 5). The coarsening process affects the stress plateau region, and creates a step that increases the stress. This simulation shows that defects can act as stress sinks, and hence defect annihilation may lead to a stress increase.

From experiments, the interrelationship between the evolving microstructure and the shear stress response was explored. While rheological models attempt to utilize these factors quantitatively to predict flow properties, this study attempts to identify the relationship between rheology and the microstructure experimentally. In Figure 5, the evolution of microstructure (AA′ section) is mapped on to the evolution of transient shear stress for a shear rate of 1s-1 at 297°C. The shear stress increased with applied shear strain till 1-2 su, where the preferred orientation of the layer planes was in the radial direction; however, size of the microstructure decreased slightly. Subsequently, a breakdown and deformation of initial microstructure was observed, which is evident from the diffuse and distorted boundaries of yellow regions at 3 su. This change of the initial microstructure results in a reduction of the stress that the material can sustain. Therefore, a peak is observed at 1-2 su. The maximum in shear stress response has also been observed for liquid crystalline polymers in the literature, and has been explained as likely resulting from the yielding of initial microstructure (Mather et al., 2000). Over the next several strain units (~10 su), the microstructure continues to yield in terms of size and orientation, and is accompanied by a decrease in shear stress. At 6 su, the deformation of initial microstructure appears to be accomplished. Subsequently, the shear stress starts to increase with increasing strain, and this upturn corresponds to a local minimum in the stress (and transient viscosity). Further shearing leads to some refinement of microstructure (shape and size) along with molecular layer-planes orientation in the flow direction.

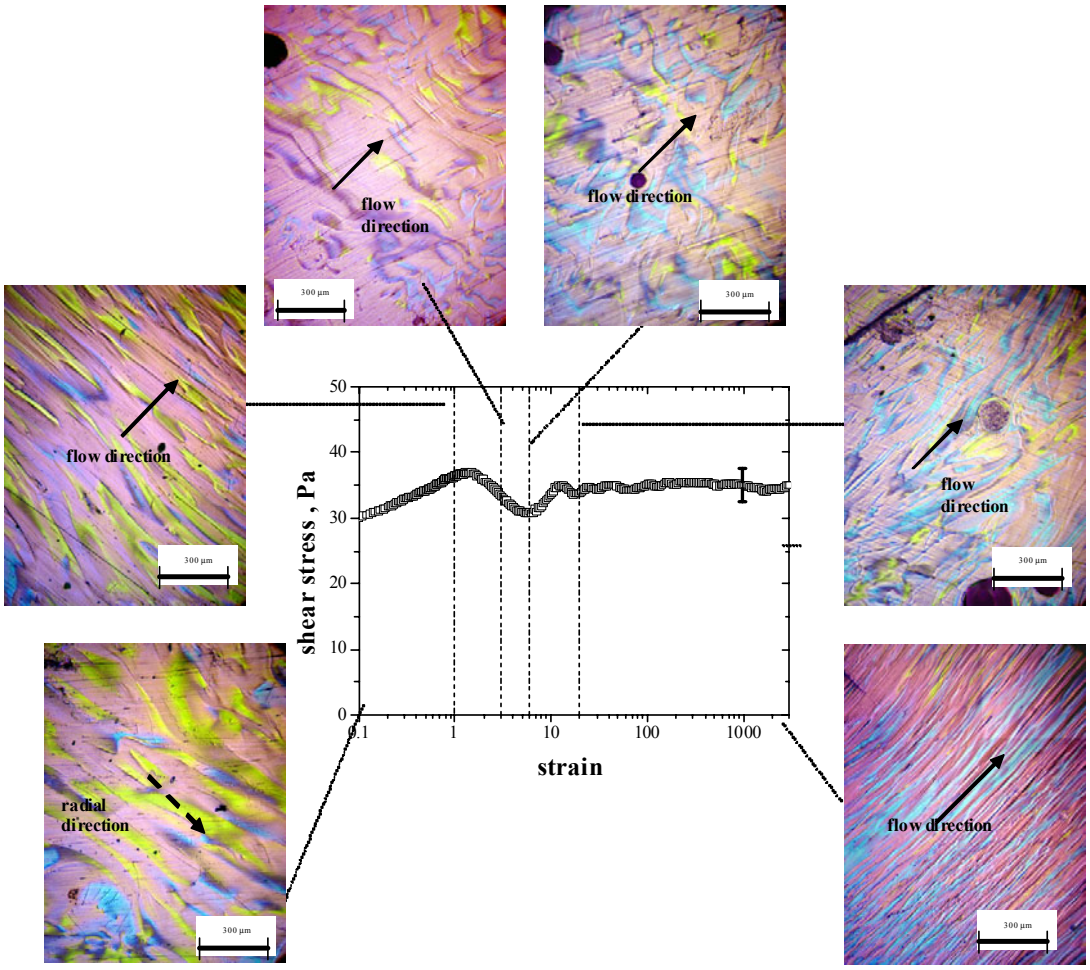

Figure 5. Rheo-structural evolution of mesophase pitch at 297°C and a shear rate of $1s^{-1}$

5. Conclusions

Based on experiments and computational results we are able to present here a systematic understanding of flow-microstructure relationship with the elucidation of texture formation in shear flow, the mechanism that control textural transformation in carbonaceous mesophases and the rheological characterization in shear start-up.

The presented multiscale theory and simulation of hydrodynamic meso and macrotexture formation is able to provide fundamental principles for control of structures and rheology in discotic liquid crystal materials.

We characterize the relation between rheological functions growth and textural transformations of carbonaceous mesophases subjected to shear start-up flow. The full impact of textural transitions on stress growth in the present model has been simplified since the positional order and geometry of the defects has been greatly restricted. In the present 1D model all splay-bend walls represent parallel and planar defects in 3D space. Nevertheless, the numerical model presented here captures important features to the much discussed rheological-textural couplings in liquid crystals.

References

Cato AD, Edie DD. 2003, Flow behavior of mesophase pitch. *Carbon* 41(7):1411–1417.

de Gennes, PG, Prost, J. 1993 The physics of Liquid Crystals, *2nd edn. Clarendon Press, Oxford*.

De'Nève T, Navard P, Kléman M. 1993. Shear rheology and shear-induced textures of a thermotropic copolyesteramide. *J Rheol* 37(3):515-529.

Edie DD. 2003, The effect of processing on the structure and properties. *In Delhaes P, editor.World of Carbon, 2(Fibers and Composites)*; CRC Press, 2003:24-46.

Fleurot O, Edie DD. 1998. Steady and transient rheological behavior of mesophase pitches. *J. Rheol* 42(4):781-793.

Grecov, D and Rey, AD. 2002. Theoretical and Computational Rheology for Discotic Nematic Liquid Crystals. *Mol Cryst Liq Cryst.* 391(1): 57-94.

Grecov, D and Rey, AD. 2003. Transient Rheology of Discotic Mesophases*, Rheologica Acta* 42(6):590-604.

Guo T, Harrison GM, Ogale AA. 2005. Transient shear rheology and rheo-optical microstructural characterization of a thermotropic liquid crystalline polymer. *Polym. Eng. Sci.* 45(2):187-197.

Imamura T, Yamada Y, Oi S, Honda H. 1978. Orientation behavior of carbonaceous mesophase spherules having a new molecular arrangement in a magnetic field. *Carbon* 16:481-486.

Kundu S, Ogale AA. Rheostructural studies on a synthetic mesophase pitch: I. Transient rheology during low-medium shear flow; *submitted to Carbon*, 2006.

Larson RG, Mead DW. 1992. Development of orientation and texture during shearing of liquid-crystalline polymers. *Liquid Crystals* 12(5):751-768.

Marrucci, G. 1984. Remarks on the viscosity of polymeric liquid crystals. In Mena B, Garcia-Rejon A, Rangel-Nafaile C, *editors. Advances in Rheology*, Vol. 1. Universidad National Autonoma De Mexico, Mexico.

Mather PT, Jeon HG, Han CD, Chang S. 2000. Morphological and Rheological Responses to Shear Start-up and Flow Reversal of Thermotropic Liquid-Crystalline Polymers. *Macromolecules* 33:7594-7608.

Picken SJ, Aerts J, Visser R, Northolt MG. 1990. Structure and rheology of aramid solutions: X-ray scattering measurements. *Macromolecules* 23:3849-3854.

Rey AD and Denn MM. 2002. Dynamical Phenomena in Liquid-Crystalline Materials. *Annu Rev Fluid Mech* 34 :233-266.

Rey AD.1990. Defect controlled dynamics of nematics liquids, *Liquid Crystals* 7(3):315-334.

Singh, AP and Rey, AD. 2000. Effect of Long Range Elasticity and Boundary Conditions on Microstructural Response of Sheared Discotic Mesophases. *J Non-Newt Fluid Mech* 94: 87 -111.

Tsuji, T and Rey, AD. 1997. Effect of long-range order on sheared liquid crystalline materials. Part I: Compatibility between tumbling behavior and fixed anchoring. *J Non-Newt Fluid Mech.* 73:127-152.

Ugaz VM, Burghardt WR. 1998. In situ X-ray scattering study of a model thermotropic copolyester under shear: evidence and consequences of flow-aligning behavior. *Macromolecules* 31:8474-8484.